IEEE Access
Multidisciplinary | Rapid Review | Open Access Journal

Received June 11, 2020, accepted July 3, 2020, date of publication July 7, 2020, date of current version August 12, 2020.

Digital Object Identifier 10.1109/ACCESS.2020.3007783

A Portable Microwave Interferometry Sensor for Permittivity Detection Based on CCMRC

SHICHANG CHEN[1], (Member, IEEE), FENG ZHOU[1], KUIWEN XU[1], (Member, IEEE), PENG ZHAO[1], (Member, IEEE), YANG YANG[2], (Senior Member, IEEE), XI ZHU[2], AND GAOFENG WANG[1], (Senior Member, IEEE)

[1]Engineering Research Center of Smart Microsensors and Microsystems, Ministry of Education, Hangzhou Dianzi University, Hangzhou 310018, China
[2]School of Electrical and Data Engineering, University of Technology Sydney, Sydney, NSW 2007, Australia

Corresponding author: Gaofeng Wang (gaofeng@hdu.edu.cn)

This work was supported in part by the Zhejiang Provincial Natural Science Foundation of China under Grant LY19F010013, in part by the Wenzhou Science & Technology Bureau Project under Grant G20190004, in part by the National Natural Science Foundation of China under Grant 61971171, and in part by the Zhejiang Provincial Key Research & Development Project under Grant 2019C04003.

ABSTRACT A portable microwave complex permittivity sensor based on the interferometry configuration is proposed. A complementary compact microstrip resonant cell (CCMRC) is applied as the sensitive element, which converts the dielectric information of the material under test (MUT) into the phase variations of its transmission coefficient. A miniaturized interferometry platform based on a down-converting mixer further translates the phase change into DC output voltage variation, which can be readily recorded with a direct readout circuit. In this context, expensive and bulky vector network analyzer is no longer needed, thereby leading to a low hardware cost. With comprehensive theoretical analysis, the material permittivity is simply extracted using a specific extrapolation algorithm. As a proof of concept, several different solid material samples with known permittivity values are used to verify the devised detection system.

INDEX TERMS Complementary compact microstrip resonant cell (CCMRC), dielectric spectroscopy, direct-conversion mixer, interferometry, microwave sensor.

I. INTRODUCTION

Permittivity contains much useful information of the material because it carries the constitutive property of matter, and the precise permittivity determination is a gray area of research. Among the permittivity sensing approaches, the microwave dielectric spectroscopy is a very attractive and desirable method due to its non-disruptive and non-contacting features. As a consequence, microwave permittivity sensors have been deployed to many different areas. In agriculture, food and pharmaceutical industries, the quality, moisture content and fermenting degrees of grains and medicines can be reflected by monitoring the permittivity variation trend with time [1]. In chemistry, the quantitative estimation of dielectric properties for polymer, gelatin and reagent can provide valuable information on the composition and structure of these chemicals [2]. In human health and biology science, dielectric constant measurement can be used for single cell detection and isolation [3], tracking the blood glucose levels of diabetes patients [4], [5] and study the relaxation of dissolved proteins [6]. Other known applications include but not limited to humidity and gas concentration detection [7], liquid composition determination [8], and so on.

Regarding to the operational principle, the microwave sensing methodology is usually built upon comparing the frequency responses of a sensitive element (SE) before and after material under test (MUT) loadings. As the most important component in a sensing system, the performance of SE significantly affects the sensitive, resolution and implementation complexity of the microwave spectroscopy platform. In the literature, sorts of structures represented by metallic waveguide [9], substrate integrated waveguide (SIW) [10], coplanar waveguide [11], microfluidic channel, passive and active microwave resonators [12] as well as metamaterial [13] have been reported. Corresponding to the diversified SE configurations, detection techniques or frequency response characterization methods have also many different forms. The most popular methods are the resonant cavity approach [14], transmission-line approach [15] and free-space approach [16]. For every individual approach, either

The associate editor coordinating the review of this manuscript and approving it for publication was Sanket Goel.

reflection or transmission variation can be used to estimate the dielectric constant.

Although the implementations of the SE and detection circuit have several different ways, an expensive vector network analyzer (VNA) is often required in order to measure the frequency response in the conventional manner. This largely prevents the spread of this technique in sensing areas where high portability and low cost are demanded. Hence, several portable design efforts have been reported recently to mitigate the dependence on bulky testing instruments. In the literature, some miniaturized on-chip VNAs are realized and applied to microwave sensor designs [17], [18]. However, these solutions are still complicated and expensive for ordinary use. Besides, some self-sustained permittivity sensors are discussed where the frequency synthesizers incorporating specifically designed voltage-controlled oscillators (VCOs) are used to characterize materials [19]–[22]. Complicated phase-locked loops (PLLs) are, nevertheless, used in these systems, and thus the hardware complexity is still quite high. Some researchers proposed an alternative methodology based on the interferometry concept to extract dielectric data [23]-[24]. However, as a heterodyne transmitter/receiver architecture is used, which comprises of two multiplier stages and two independent signal sources, the high system complexity has not been fully resolved. Later on, the direct-conversion configurations, as well as interferometry reflectometers, were proposed to replace the heterodyne systems, and the corresponding extraction algorisms were updated accordingly [13], [25]–[28].

In this study, a highly sensitive complementary compact microstrip resonant cell (CCMRC) is applied as SE, which transforms the MUT permittivity into its phase variation of transmission characteristics. This is further converted into the change of output voltage of the mixer in a direct-conversion sensor. Low-cost digital voltmeter rather than expensive VNA is adequate to extract the material permittivity information.

The remaining of this paper is organized as follows: Section II introduces the operational theory and configuration of the proposed microwave sensor and the implementation of some key components. In Section III, the simulated and experimental results of the whole sensing system are presented, followed by a conclusion in section IV.

II. PROPOSED SENSOR BASED ON INTERFEROMETRY

A. SENSOR ARCHITECTURE AND DESIGN RULES

The illustrative diagram of the proposed permittivity sensor based on interferometry architecture is shown in Fig. 1. It is comprised of two independent paths. The upper path, herein named as the RF path, contains a sensitive element (SE) and a voltage-controlled phase shifter (VCPS). The lower path consists of a phase compensation line (PCL), is herein called the LO path. These two paths are connected to a power divider at the input side and a down-converting mixer at the output side. The operational principle of the system is summarized below.

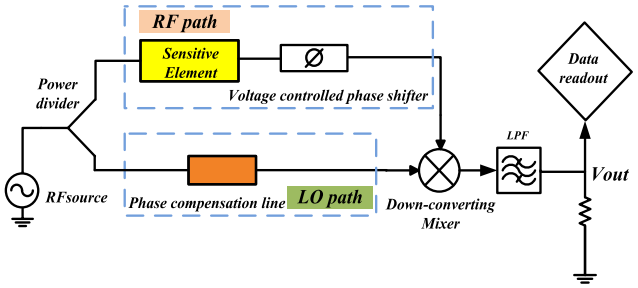

FIGURE 1. Illustrative diagram of the proposed permittivity sensor.

The input RF excitation is distributed into the two branches that drive the RF and LO paths, respectively, through the power divider. As the RF and LO ports of the down-converting mixer have identical frequencies, it produces a DC voltage whose value is related to the magnitudes and relative phases of the RF and LO excitations. To be detailed, suppose the signal injected into the RF path is a pure cosine wave, which takes the following form,

$$v_{RF} = A_{RF}\cos(\omega_s t). \tag{1}$$

where A_{RF} and ω_s are the amplitude and angular frequency of the excitation, respectively. For the sake of simplicity, the initial phase of the input RF signal is assumed to be zero. On the other hand, as the LO signal has the same operating frequency as the RF one, it can be expressed as,

$$v_{LO} = A_{LO}\cos(\omega_s t + \varphi). \tag{2}$$

where A_{LO} and φ represent the amplitude and relative phase of the LO signal, respectively. According to the operation principle of a down-converter, the output of the mixer can be calculated as follows,

$$\begin{aligned} V_{OUT} &= K_M \times A_{RF}\cos(\omega_s t) \times A_{LO}\cos(\omega_s t + \varphi) \\ &= \frac{1}{2}K_M A_{RF} A_{LO}[\cos(2\omega_s t + \varphi) + \cos(-\varphi)]. \end{aligned} \tag{3}$$

where K_M represents the conversion gain of mixer. It is readily seen that if the RF and LO signals are treated as pure sinusoidal curves and their harmonic mixings are ignored, the mixer output contains a DC component whose value is closely dependent on the RF and LO amplitudes, as well as their relative phase φ,

$$V_{DC,0} = \frac{1}{2}K_M A_{RF} A_{LO}\cos(-\varphi). \tag{4}$$

In this particular design, φ is chosen to be 90° by tuning the length of the PCL in the LO path for the initial status (without MUT loading). According to (4), one can readily see that the output DC voltage is zero under this setting, regardless of the values of A_{LO}, A_{RF} and K_M.

When the SE is exposed to a specific material, it is intuitive that its frequency characteristics will change accordingly. In other words, some magnitude or phase deviations will

apply to the RF path. As a consequence, the expression of RF signal will be changed to,

$$v'_{RF} = A'_{RF}\cos(\omega_s t - \theta_{mut}). \tag{5}$$

Similar as before, A_{RF}' is the instantaneous signal amplitude, while θ_{mut} is the additional phase shift induced by MUT. As the LO path remains intact, the DC voltage of mixer output (defined as $V_{DC,1}$) will be different subsequently,

$$V_{DC,1} = \frac{1}{2}K_M A'_{RF} A_{LO}\cos(-\theta_{mut} + 90^\circ) \tag{6}$$

However, the exact value of θ_{mut} cannot be obtained directly from (6) as $V_{DC,1}$ is jointly determined by several parameters. Therefore, an additional phase shift ψ_{ps} is added to the RF path by a VCPS whose topology will be given later. In this context, the mixer output (defined as $V_{DC,2}$) is updated to,

$$V_{DC,2} = \frac{1}{2}K_M A'_{RF} A_{LO}\cos(-\theta_{mut} - \psi_{ps} + 90^\circ) \tag{7}$$

From (7), it is readily seen that a zero DC output can be retrieved when ψ_{ps} approaches $-\theta_{mut}$. Alternatively speaking, as long as the ψ_{ps} value at the zero output condition is known, the MUT related phase-shifting is also obtained. Referring to previous works, by obtaining the phase variation of the SE before/after MUT loadings, the material information can be extracted [20]–[22]. These constitute the theoretical fundamentals of the proposed work. It needs to emphasize that, although zero output voltage is applied as the phase matching condition of the VCPS and MUT, the peak output voltage can also be utilized as the judgment criteria according to (4) and (7). For this, the RF and LO signal should be made in phase initially by tuning the length of the PCL.

B. SENSITIVE ELEMENT DESIGN

With the overall sensor structure outlined and the operational principle given, the next steps are to realize the essential components in the proposed configuration. The details will be introduced in the following parts.

In this work, an energy band-gap (EBG) structure named CCMRC is used for SE design. As is shown in Fig. 2(a), the so-called CCMRC is a quasi-lumped structure with a specific pattern etched on a rectangular patch and shorting pins added at the edges of the cell [29]. The pins (vias) provide short circuit conditions for the equivalent *λ/4* resonators and provides cross-coupling between non-adjacent resonators. Due to these structural features, the CCMRC is mirror opposite to the well-known compact microstrip resonant cell (CMRC) in both pattern and frequency characteristics. In other words, contrast to the band-stop characteristics of the CMRC [30]-[32], the CCMRC features a typical band-pass filtering characteristics. In addition, due to the special pattern of the CCMRC, its frequency response can be readily perturbed by external materials, which makes it a highly sensitive element. Fig. 2(b) gives the simulated electrical field distribution in HFSS software. Herein, the investigation frequency is set to 5 GHz.

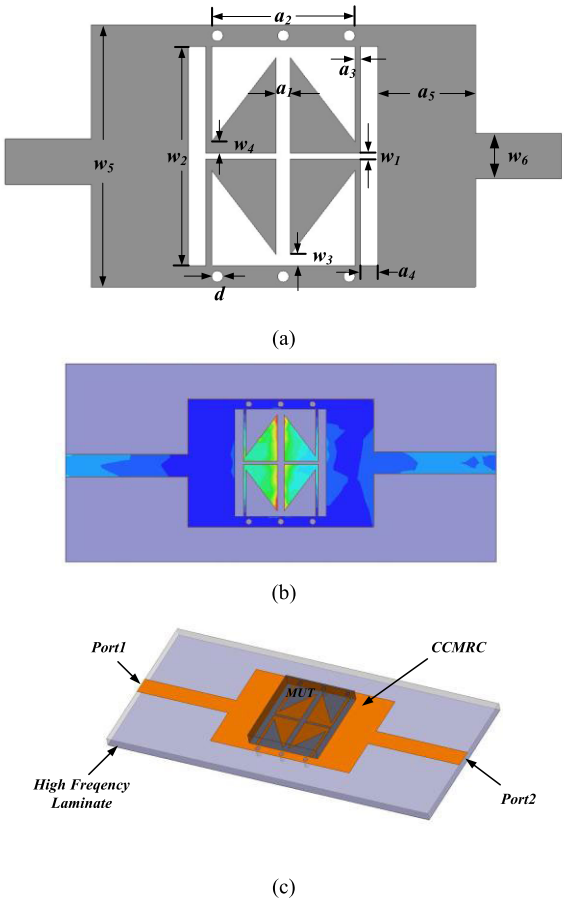

FIGURE 2. (a) Diagram of a CCMRC unit. (b) Simulated field distribution of a CCMRC unit. (c) 3D illustration of the CCMRC based sensitive element.

Fig. 2(c) depicts the three-dimensional (3D) illustration of the proposed SE. Port 1 and port 2 are the input and output of the SE, respectively. The MUT sample is placed above the hallow pattern of CCMRC, whose function will be discussed in following section. In order to reduce unwanted reflections, the microstrip widths are carefully tuned to have 50 Ω port impedances when no material is applied.

As is well known, the dielectric constants of most materials are complex and frequency-dependent, and can be expressed in a complex formula as $\varepsilon_r(\omega) = \varepsilon'_r(\omega) - j\varepsilon''_r(\omega)$, where $\varepsilon'_r(\omega)$ and $\varepsilon''_r(\omega)$ are the real and imaginary parts, respectively. The real part represents the ability of the material to store energy, while the imaginary part represents the material loss.

Fig. 3(a) depicts the simulated transmission coefficient S21 of a CCMRC exposed to a MUT with different $\varepsilon'_r(\omega)$ ranging from 2 to 12 with a spacing of 2. It is readily seen that the frequency response of CCMRC changes with different ε_r values. Besides, the positions of S21 peaks can be adjusted by tuning the dimension of the unit, as illustrated in [32]. Moreover, the corresponding phases for the proposed SE with different MUT permittivity and dimensions are shown in Fig. 3(b). As one can see, when the MUT dimension increases, the induced phase-shifting value also increases. However, as shown in Fig. 2(b), most of the electric field is

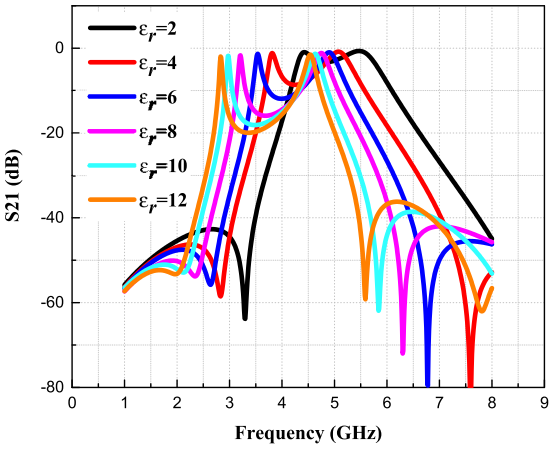

(a)

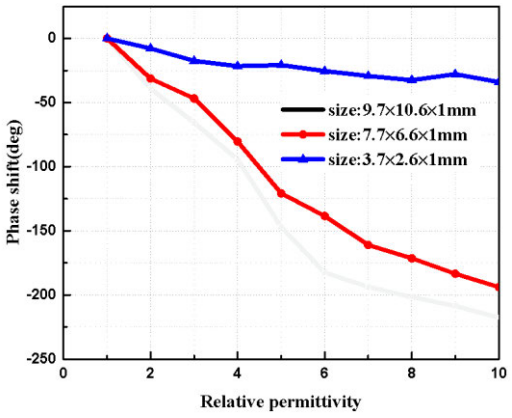

(b)

FIGURE 3. Simulated S21 of CCMRC under a MUT with different ε_r values: (a) Magnitude and (b) phase variations with respect to different MUT permittivity and dimensions for the frequency of 5 GHz.

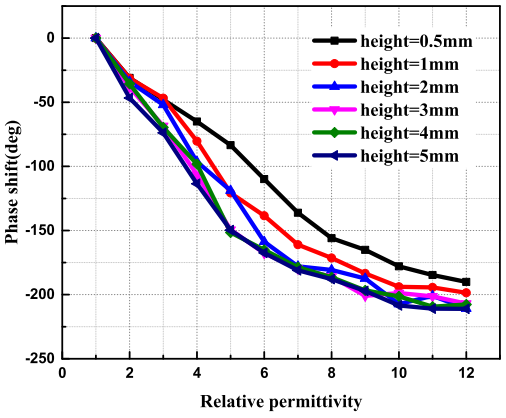

FIGURE 4. Simulated SE phase shift against MUT permittivity and height.

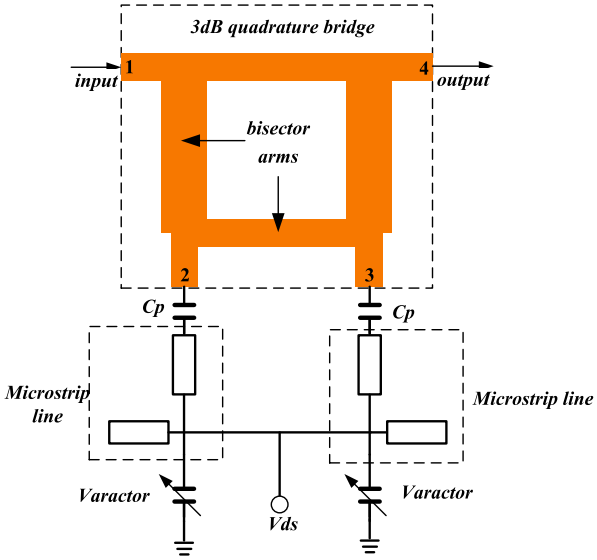

FIGURE 5. Schematic diagram of proposed voltage controlled phase shifter.

confined in the center part of CCRMC which leads to large perturbation. As a result, the width and length of MUT are set to be exactly the same as the hallow pattern of CCMRC to achieve good balance between performance and MUT size. In addition, as the MUT size is established, the induced phase shift has a one-to-one correspondence with $\varepsilon_r'(\omega)$. Inspired by this, one can acquire the $\varepsilon_r'(\omega)$ information by extracting the phase of CCMRC element.

For better demonstration, the simulated phase response of SE versus the MUT height is shown in Fig. 4. It is readily seen that the material height has some influence on the phase shift value. This is because when the height increases, more electric field is confined in the MUT. In addition, the phase shift will become constant when a certain value is reached. As shown in Fig. 4, this value is roughly 4 mm for this particular CCMRC structure. Therefore, to have an accurate sensing result, all materials used in this particular work are prepared with a fixed height of 1 mm, a value easy for sample preparations. Nevertheless, the one-to-one correspondence between MUT permittivity and SE phase variation still holds for a different MUT height. Finally, the size of MUT is 6.6 mm × 7.7 mm × 1 mm, and the imaginary part of material is neglected for analysis simplicity ($\varepsilon_r''(\omega) = 0$).

C. VOLTAGE CONTROLLED PHASE SHIFTER DESIGN

According to the above analysis and equation (7), a phase shifter with tunable shifting amount is required to compensate for the phase variation caused by MUT loading. Accordingly, a VCPS is designed, as shown in Fig. 5.

This proposed VCPS, a 3-dB quadrature bridge phase shifter alternatively named, is built upon an orthogonal bridge with two vertical bisector arms. All the lines are 90-degree long at the center frequency, 5 GHz in this particular work. Port 1 is the input terminal, while port 2 is the straight through terminal for the quadrature coupler. Moreover, port 3 and port 4 are the coupling and isolated ends, respectively. The input signal is divided into two ways through the bisector arms, and enters port 2 and port 3 connecting to two varactors, respectively. The signal injected to these two ports will be reflected by the varactors (ideally pure reactances)

because of impedance mis-matchings. Assume that the phase of the reflected signal from port 2 is Ψ which is determined by the varactor susceptance. The reflected signal re-enters the 3-dB quadrature bridge, which is distributed further into port 1 and 4, with the corresponding phases of $\Psi - 90°$ and $\Psi - 180°$, respectively. Similarly, if the two varactors are assumed identical in terms of size and biasing voltage, the phase of the reflected signal from port 3 is $\Psi - 90°$, and the phase of the picked signal at ports 1 and 4 are now $\Psi - 270°$ and $\Psi - 180°$, respectively. It is readily seen that the reflected signals seen at port 1 are out-of-phase, counteracting each other. In contrast, that for port 4 are in-phase superposed. As a consequence, the input signal at port 1 is completely transmitted to port 4 due to the reflections that happened at the varactors, and the relative phase-shifting amount is closely related to the reactances of the varactors (Ψ value). As varactor reactances are dependent on biasing voltages, the phase of the output signal can be therefore controlled by giving different biasing voltages V_{ds}.

In this particular work, to have a large detection range of dielectric constant values, at least 180° phase-shifting capability is needed, conforming to the periodic feature of a sinusoidal function. For this reason, two identical matching networks made up of a series and a shunt microstrip lines are added between each varactor and its corresponding bridge port, respectively. Their functionality is to increase the phase shift range and compensate for the linearity of the phase shifter. The varactors used herein are SMV1232 from SKYWORKS with a capacitance tunable range from 0.75 pF to 4 pF corresponding to a control voltage from 0 V to 15 V.

Fig. 6 shows the simulation results of the proposed VCPS as a function of biasing voltage in Keysight ADS, with the varactor models provided by the manufacture. One can see that the devised VCPS can provide a monotonically growing relationship between phase-shifting amount and the bias voltage V_{ds}. And its shifting range covers $-170°$ to 40°, accounting for an absolute value larger than 180°. In addition, the detail shifting amount has one-to-one correspondence to V_{ds}. From the circuit design aspect, one can have the phase-shifting value induced by VCPS by simply measuring V_{ds}, and further extract the permittivity information of MUT according to the aforementioned principles. A bulky and expensive vector network analyzer (VNA) generally required in conventional schemes is therefore unnecessary, which will help to reduce the system monetary expense significantly.

Moreover, it needs to emphasize that although the loss accompanying the phase shifter is not trivial (about 1.6 dB), as shown in Fig. 6(b), its effect on sensing result can be neglected as the detection is independent to the magnitude of the RF signals before/after the MUT placements according the analysis given above.

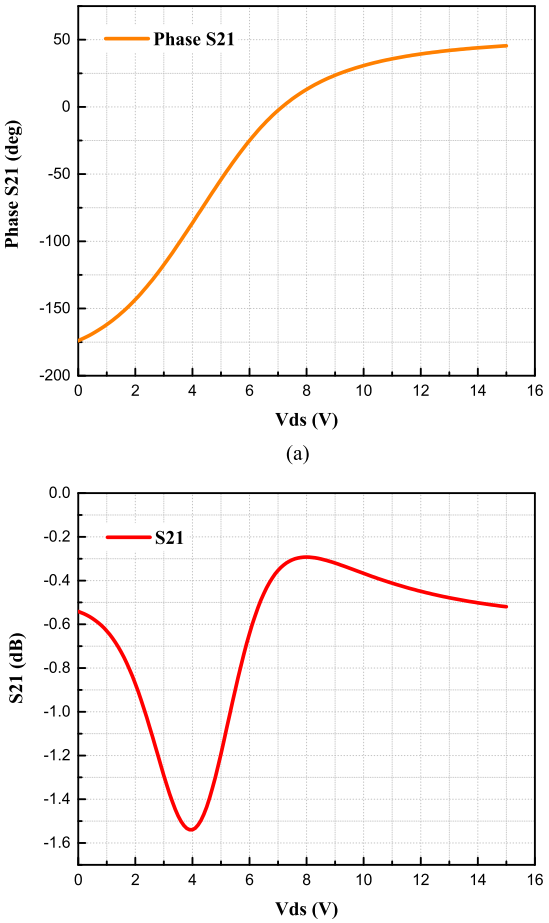

FIGURE 6. Simulation performance of the proposed VCPS under different biasing voltage at 5 GHz: (a) Phase shift amount (b) transmission loss.

III. SIMULATION AND MEASUREMENT RESULTS

A. SIMULATIONS

To verify the effectiveness of the proposed architecture, the CCMRC unit and the whole circuit are simulated in different ways. First of all, the dimensions of the CCMRC are optimized in EM software to have a 5 GHz center frequency with no material loading. The Rogers 4350 laminate with a dielectric constant of 3.66 and a thickness of 0.762 mm is used as substrate. In addition, the characteristic impedance of the microstrip connecting to the two ports are tuned to be 50 Ω, reducing reflections and loss when CCMRC is connected to other peripheral circuitry. The dimensions of the optimized CCMRC structure are listed in Table 1.

Next, the remaining building components in the devised system are modelled in Keysight ADS and then the overall structure simulation is performed. Note that the data corresponding to the CCMRC with different MUTs are imported into ADS for co-simulation.

The simulated output DC voltages of the down-mixer as a function of the biasing voltage of varactors V_{ds} in the VCP are shown in Fig. 7. The V_{ds} value is scanned from 0 V to 15 V. For the case that no MUT is added (pink line), according to formula (5)-(7), the relationship between the DC voltage of mixer and the phase-shifting value provided by the VCPS is a cosine function. Since the relation between the phase-shifting value and the biasing voltage is not completely linear, a quasi-cosine rather than a pure cosine profile

TABLE 1. Parameters Of CCMRC.

w_1 (mm)	0.2	a_1 (mm)	0.5
w_2 (mm)	7.7	a_2 (mm)	5
w_3 (mm)	0.4	a_3 (mm)	0.2
w_4 (mm)	0.4	a_4 (mm)	0.6
w_5 (mm)	9.2	a_5 (mm)	3.4
w_6 (mm)	1.6	d (mm)	0.4

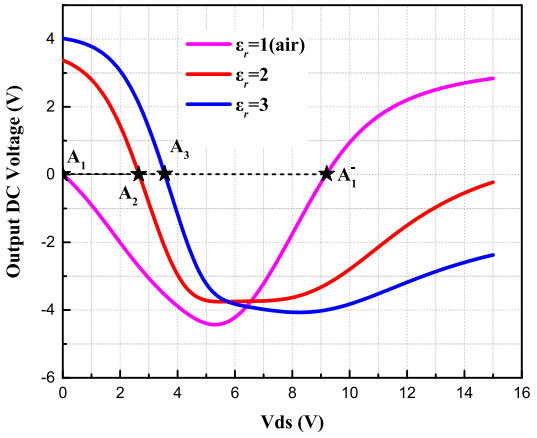

FIGURE 7. Relationship between biasing voltage V_{ds} for VCPS and mixer output DC voltage.

is obtained. However, its cosine-like curve still proves the successful operation of the down-mixer. In addition, there exist two points (A and A^-) where the output DC voltage is 0 V when the biasing voltage V_{ds} increases for each case with different MUT placement. These two points correspond to conditions at which the RF and the LO branches present 90° and 270° phase differences, respectively. According to the operational principle mentioned above, point A of great significance for the permittivity-voltage determination. And its position can be adjusted by tuning the length of the phase compensation line in the LO branch. In this design, the corresponding V_{ds} for point A is set to zero volts deliberately for the sake of simplicity during analysis.

Moreover, it is readily seen that the varactor bias voltage corresponding to zero output shifts to higher values when the dielectric constant of MUT increases (marked with $A_1 - A_3$). A one-to-one correspondence is expected. Consequently, it is intuitive that when the bias voltage is measured, the corresponding dielectric constant can be easily obtained as long as their relationship is extracted. This can be done through the multi-group data simulation and curve fitting.

B. HARDWARE IMPLEMENTATION AND MEASUREMENTS

To realize the proposed sensor, an off-the-shelf passive mixer HMC219B from Analog Device Inc is used. Its operating frequency range is 2.5 GHz to 7 GHz, which satisfies the 5 GHz operating frequency of the sensor. The RF and LO input powers are 25 dBm and 27 dBm, respectively. The LO power

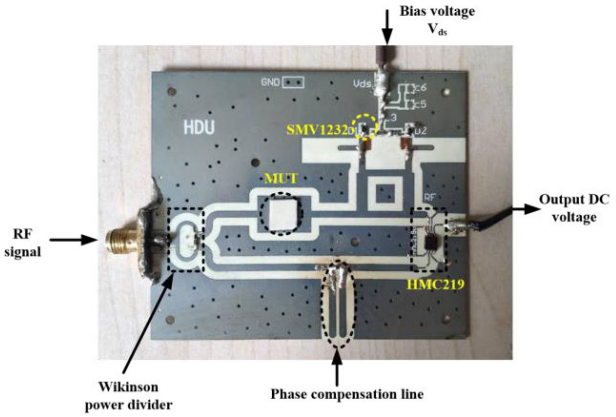

FIGURE 8. Photograph of implemented microwave interferometry sensor for permittivity detection based on CCMRC.

is slightly larger in order to drive the mixer in a full capacity. Accordingly, an uneven Wilkinson power splitter is implemented at the input side, which distributes the input signals into the RF and the LO branches. The 5 GHz excitation is produced by the signal generator SMW200A from Rohde & Schwarz. Of course, if self-sustained operation is required, the driving signal can be easily generated by a PLL-based frequency synthesizer [21], [22].

Moreover, to compensate for the uncertainty caused by the differences between the real components and their models as well as fabrication tolerance, a long PCL consisting of two adjacent parallel microstrip lines are aligned in the prototype circuit, as shown in Fig. 8. The line widths are set to 1.6 mm, corresponding to 50 Ohm characteristic impedances for the specific laminate on which the sensor is fabricated. The real length of PCL is tuned by changing the position of the decoupling capacitor. As mentioned before, a 90-degree phase difference between the two branches is chosen in the initial state (without MUT loading), which subsequently produces zero output voltage.

The measured and simulated output voltages versus the varactor controlled voltage V_{ds} are compared in Fig. 9(a), where no MUT is introduced. Note that the two curves are slightly different, and the measured curve is steeper than the simulated one when V_{ds} is below 3 V. In other words, the phase-shifting provided by the actual VCPS is larger than the simulation value in this particular voltage range. This difference can be attributed to several reasons such as the model inaccuracy regarding the varactor and mixer, fabrication tolerance and etc. For example, the down-mixer used for simulation is assumed to have constant conversion gain, while for a real device, its gain varies slightly under different LO power, harmonic impedance or working temperature. According to previous literature [19]–[21], these performance deviations will not impede the execution of the proposed architecture as the detailed voltage-permittivity relationship can be readily extracted using curve fitting technique if a set of MUT samples with known permittivity are used for the system calibration. For demonstration, four different dielectric laminates, Rogers 5880, Rogers 4350B,

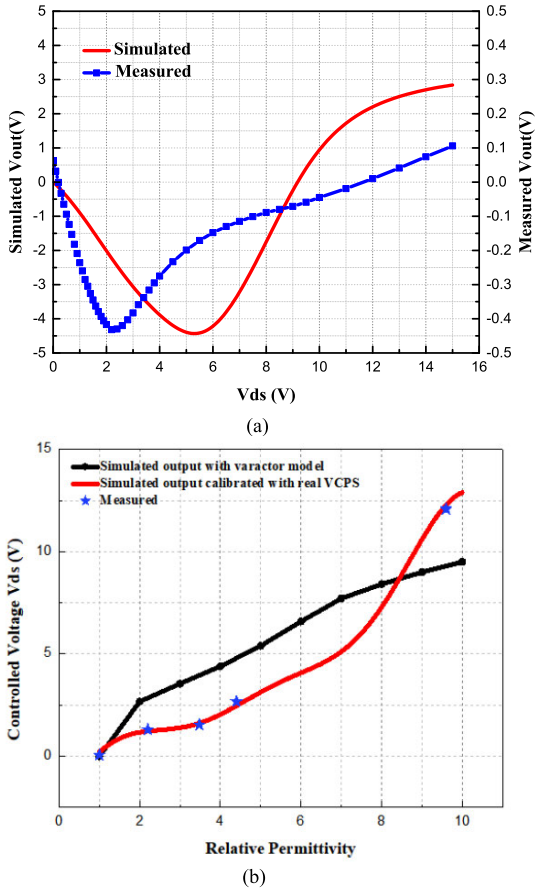

FIGURE 9. Measured and simulated: (a) relationship between bias voltage *Vds* and output DC voltage with no MUT (b) bias voltage versus material dielectric constant.

FR4 and a ceramic with relative permittivity of 2.2, 3.48, 4.4, 9.6 and loss tangent of 0.009, 0.004, 0.02, 0.025 are applied in measurements. In particular, as it is somewhat difficult to prepare MUTs with large height, these laminates are polished carefully to a height of 1 mm, in accordance with the simulation setup introduced previously. The width and length of MUTs are still kept as 7.6 mm × 6.6 mm, respectively. Their corresponding values of the V_{ds} are recorded as 1.302 V, 1.691 V, 2.670 V and 12.08 V, respectively. Herein, the Keysight 34461A digital multi-meter is used to measure the system output voltages. The measurements are performed for four times by switching the system on and off repeatedly and recording the output each time, the final data takes the average value. It is found that the results are quite constant, with a vibration within ±1 mV, a fine resolution confined by the digital multi-meter. Besides, it need to emphasize that off-the-shelf analog-to-digital converters (ADC) can also be used to readout the output voltage, if necessary. And the proposed sensor architecture can be modified for different applications such as liquid sensing by appropriate structural adjustment of the CCMRC unit, while the other circuitry may remain as the present form.

Fig. 9(b) depicts the profiles of the simulated (the black dotted curve) and measured (discrete points marked with

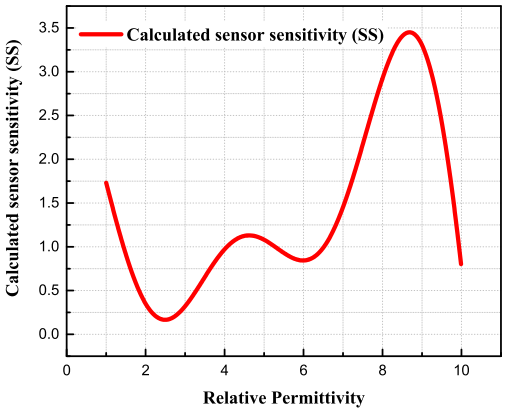

FIGURE 10. The calculated sensor sensitivity (SS) versus MUT permittivity of the proposed sensor.

star symbols) VCPS controlling voltage as a function of the relative permittivity of the MUT. As one can readily note, although the absolute voltage magnitudes do not match, the measured voltage has similar variation trend against the MUT permittivity. These are mainly caused by the differences between real devices and the simulation models. To further demonstrate the accuracy of the proposed sensor, the measured data shown in Fig. 9(a) is used to calibrate out the influence caused by the above mentioned difference between practical devices and their model in simulations. The calibrated curve is added in the same figure (the red curve). One can easily note that after this calibration, the measurement results approximate the simulated ones greatly.

Note that the relationship between the relative permittivity and the controlled voltage is nonlinear. Therefore, a nonlinear fitting is conducted in MATLAB to form an approximated equation:

$$V_{ds} = a_0 + a_1\cos(\omega\varepsilon_r) + b_1\sin(\omega\varepsilon_r) + a_2\cos(2\omega\varepsilon_r) + b_2\sin(2\omega\varepsilon_r) + a_3\cos(3\omega\varepsilon_r) + b_3\sin(3\omega\varepsilon_r) \quad (8)$$

and these fitting constants are obtained as $a_0 = 3.302$, $a_1 = -5.991$, $a_2 = -0.8686$, $a_3 = 1.277$, $\omega = 0.395$, $b_1 = -1.57$, $b_2 = 3.7$, $b_3 = 0.5827$, respectively. Based on this extracted equation, and the measured biasing voltage V_{ds} of the materials with known dielectric constant as 2.2, 3.48, 4.4, and 9.6, the error rates corresponding to the four MUTs are calculated as 2.7%, 3.7%, 3.1% and 0.8%, respectively. The discrepancies between simulation and measurement can be attributed to the gaps between the CMRC and the MUT, fabrication tolerance as well as the material misalignment.

Regarding to the sensor sensitivity (SS), which is commonly defined as the ratio between the output variation and the dielectric permittivity variation as SS= $\Delta V_{ds}/\Delta\varepsilon_r$ [34]. Accordingly, the SS value can be readily extracted by calculating the slope of the red curve corresponding to the real VCPS in this particular design, as shown in Fig. 9(b). Based on (8), by performing a simple derivative operation, the SS

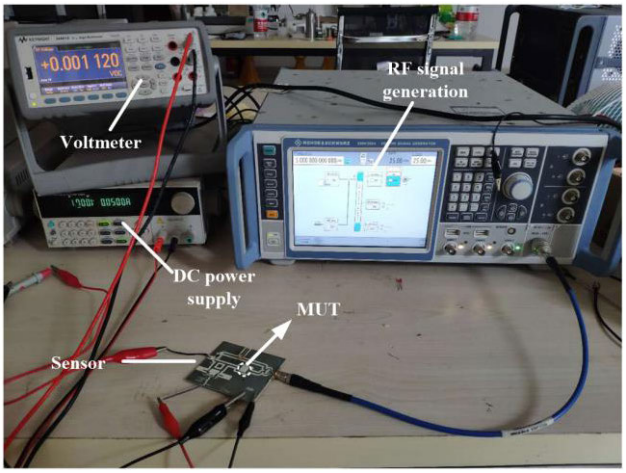

FIGURE 11. The measurement setup of the proposed sensor.

TABLE 2. Comparison to other works.

Ref	Freq (GHz)	Detection capability	Measurement technique for reference	Error rate
[13]	4.2-8	ε'_r and ε''_r of liquids	Multimeter	1.1% for ε'_r 1.6% for ε''_r
[15]	1-8	ε'_r of low-loss materials	VNA	5% for ε'_r
[19]	7-9	ε'_r of liquids	Multimeter	3.7% for ε'_r and ε''_r
[21]	3.7	ε'_r of liquids	Multimeter	4% for ε'_r
[22]	1.24	ε'_r of solids	Multimeter	N/A
[33]	2.6	ε'_r and ε''_r of solids	VNA	5.05% for ε'_r
[34]	0.8-2.2	ε'_r and ε''_r of solids	VNA	3.9% for ε'_r 4.5% for ε''_r
This work	5	ε'_r of solids	Multimeter	3.7% for ε'_r

can be expressed as,

$$SS = -a_1\omega\sin(\omega\varepsilon_r) + b_1\omega\cos(\omega\varepsilon_r) - 2a_2\omega\sin(2\omega\varepsilon_r) + 2b_2\omega\cos(2\omega\varepsilon_r) - 3a_3\omega\sin(3\omega\varepsilon_r) + 3b_3\omega\cos(3\omega\varepsilon_r) \quad (9)$$

after substituting the aforementioned fitting constants into it, the sensitivity is calculated between 0.166 and 3.449 after simple mathematical derivation, as shown in Fig. 10. The minimum value happens for the permittivity of 2.5, while the MUT permittivity corresponding to maximum sensitivity is around 8.7. Besides, as the voltage resolution of the digital multimeter is 1 mV, the theoretical minimal detectable permittivity variation is therefore calculated to be 0.006 by dividing the voltage resolution with the reciprocal of the obtained sensitivity. As one can readily see, very tiny permittivity variation can be monitored using the proposed sensor. Table 2 compares the performance of the proposed sensor in this work with some relevant works published recently. And Fig. 11 shows the measurement setup in the lab.

IV. CONCLUSION

In this work, a novel microwave dielectric constant sensor was proposed by virtue of the interferometry concept. The CCMRC structure was applied as the sensing element, which is high in sensitivity, compact in size and compatible to the planar circuits. Based on a down-converting mixer, the material permittivity was detected precisely by simply measuring the bias voltage of a microwave voltage-controlled phase shifter. Therefore, the detection speed and sensitivity were greatly improved. The largest error rate is below 3.7 %. In the meantime, the system complexity and realization cost were largely reduced.

REFERENCES

[1] M. P. Abegaonkar, R. N. Karekar, and R. C. Aiyer, "Miniaturized nondestructive microwave sensor for chickpea moisture measurement," *Rev. Sci. Instrum.*, vol. 70, no. 7, pp. 3145–3149, Jul. 1999.
[2] R. Baw and J. Finkelsetein, "Lab on chip," *Nature*, vol. 442, no. 7101, pp. 367–418, Jul. 2006.
[3] K. Grenier, D. Dubuc, T. Chen, F. Artis, T. Chretiennot, M. Poupot, and J.-J. Fournie, "Recent advances in microwave-based dielectric spectroscopy at the cellular level for cancer investigations," *IEEE Trans. Microw. Theory Techn.*, vol. 61, no. 5, pp. 2023–2030, May 2013.
[4] X. Xiao and Q. Li, "A noninvasive measurement of blood glucose concentration by UWB microwave spectrum," *IEEE Antennas Wireless Propag. Lett.*, vol. 16, pp. 1040–1043, 2017.
[5] A. K. Jha, Z. Akhter, N. Tiwari, K. T. M. Shafi, H. Samant, M. J. Akhtar, and M. Cifra, "Broadband wireless sensing system for non-invasive testing of biological samples," *IEEE J. Emerg. Sel. Topics Circuits Syst.*, vol. 8, no. 2, pp. 251–259, Jun. 2018.
[6] T. H. Basey-Fisher, S. M. Hanham, H. Andresen, S. A. Maier, M. M. Stevens, N. M. Alford, and N. Klein, "Microwave debye relaxation analysis of dissolved proteins: Towards free-solution biosensing," *Appl. Phys. Lett.*, vol. 99, no. 23, Dec. 2011, Art. no. 233703.
[7] Z. Abbasi, P. Shariaty, M. Nosrati, Z. Hashisho, and M. Daneshmand, "Dual-band microwave circuits for selective binary gas sensing system," *IEEE Trans. Microw. Theory Techn.*, vol. 67, no. 10, pp. 4206–4219, Oct. 2019.
[8] W. Withayachumnankul, K. Jaruwongrungsee, C. Fumeaux, and D. Abbott, "Metamaterial-inspired multichannel thin-film sensor," *IEEE Sensors J.*, vol. 12, no. 5, pp. 1455–1458, May 2012.
[9] K. Saeed, R. D. Pollard, and I. C. Hunter, "Substrate integrated waveguide cavity resonators for complex permittivity characterization of materials," *IEEE Trans. Microw. Theory Techn.*, vol. 56, no. 10, pp. 2340–2347, Oct. 2008.
[10] N. K. Tiwari, A. K. Jha, S. P. Singh, Z. Akhter, P. K. Varshney, and M. J. Akhtar, "Generalized multimode SIW cavity-based sensor for retrieval of complex permittivity of materials," *IEEE Trans. Microw. Theory Techn.*, vol. 66, no. 6, pp. 3063–3072, Jun. 2018.
[11] H.-W. Wu, "Label-free and antibody-free wideband microwave biosensor for identifying the cancer cells," *IEEE Trans. Microw. Theory Techn.*, vol. 64, no. 3, pp. 982–990, Mar. 2016.
[12] M. Bakhshiani, M. A. Suster, and P. Mohseni, "A 9 MHz-2.4 GHz fully integrated transceiver IC for a microfluidic-CMOS platform dedicated to miniaturized dielectric spectroscopy," *IEEE Trans. Biomed. Circuits Syst.*, vol. 9, no. 6, pp. 849–861, Dec. 2015.
[13] A. Pourghorban Saghati, J. S. Batra, J. Kameoka, and K. Entesari, "A metamaterial-inspired wideband microwave interferometry sensor for dielectric spectroscopy of liquid chemicals," *IEEE Trans. Microw. Theory Techn.*, vol. 65, no. 7, pp. 2558–2571, Jul. 2017.

[14] A. W. Kraszewski, S. O. Nelson, and T.-S. You, "Use of a microwave cavity for sensing dielectric properties of arbitrarily shaped biological objects," *IEEE Trans. Microw. Theory Techn.*, vol. 38, no. 7, pp. 858–863, Jul. 1990.
[15] P. M. Narayanan, "Microstrip transmission line method for broadband permittivity measurement of dielectric substrates," *IEEE Trans. Microw. Theory Techn.*, vol. 62, no. 11, pp. 2784–2790, Nov. 2014.
[16] X. Faget, A. Litman, E. Dieudonne, S. Enoch, and N. Mallejac, "Free-space characterization of the permeability of inhomogeneous magneto-dielectric materials," *IEEE Trans. Microw. Theory Techn.*, vol. 65, no. 12, pp. 5035–5045, Dec. 2017.
[17] I. Nasr, J. Nehring, K. Aufinger, G. Fischer, R. Weigel, and D. Kissinger, "Single- and dual-port 50-100-GHz integrated vector network analyzers with on-chip dielectric sensors," *IEEE Trans. Microw. Theory Techn.*, vol. 62, no. 9, pp. 2168–2179, Sep. 2014.
[18] J. Nehring, M. Schutz, M. Dietz, I. Nasr, K. Aufinger, R. Weigel, and D. Kissinger, "Highly integrated 4-32-GHz two-port vector network analyzers for instrumentation and biomedical applications," *IEEE Trans. Microw. Theory Techn.*, vol. 65, no. 1, pp. 229–244, Jan. 2017.
[19] A. A. Helmy, H.-J. Jeon, Y.-C. Lo, A. J. Larsson, R. Kulkarni, J. Kim, J. Silva-Martinez, and K. Entesari, "A self-sustained CMOS microwave chemical sensor using a frequency synthesizer," *IEEE J. Solid-State Circuits*, vol. 47, no. 10, pp. 2467–2483, Oct. 2012.
[20] O. Elhadidy, M. Elkholy, A. A. Helmy, S. Palermo, and K. Entesari, "A CMOS fractional-*N* PLL-based microwave chemical sensor with 1.5% permittivity accuracy," *IEEE Trans. Microw. Theory Techn.*, vol. 61, no. 9, pp. 3402–3416, Sep. 2013.
[21] S. Chen, M. Guo, K. Xu, P. Zhao, Y. Hu, L. Dong, and G. Wang, "A dielectric constant measurement system for liquid based on SIW resonator," *IEEE Access*, vol. 6, pp. 41163–41172, 2018.
[22] S. Chen, M. Guo, K. Xu, P. Zhao, L. Dong, and G. Wang, "A frequency synthesizer based microwave permittivity sensor using CMRC structure," *IEEE Access*, vol. 6, pp. 8556–8563, 2018.
[23] M. Bakhshiani, M. A. Suster, and P. Mohseni, "A broadband sensor interface IC for miniaturized dielectric spectroscopy from MHz to GHz," *IEEE J. Solid-State Circuits*, vol. 49, no. 8, pp. 1669–1681, Aug. 2014.
[24] J.-C. Chien, M. Anwar, E.-C. Yeh, L. P. Lee, and A. M. Niknejad, "A 1-50 GHz dielectric spectroscopy biosensor with integrated receiver front-end in 65nm CMOS," in *IEEE MTT-S Int. Microw. Symp. Dig.*, Jun. 2013, pp. 1–4.
[25] A. A. Helmy, S. Kabiri, M. Moslehi Bajestan, and K. Entesari, "Complex permittivity detection of organic chemicals and mixtures using a 0.5-3-GHz miniaturized spectroscopy system," *IEEE Trans. Microw. Theory Techn.*, vol. 61, no. 12, pp. 4646–4659, Dec. 2013.
[26] M. M. Bajestan, A. A. Helmy, H. Hedayati, and K. Entesari, "A 0.62-10 GHz complex dielectric spectroscopy system in CMOS," *IEEE Trans. Microw. Theory Techn.*, vol. 62, no. 12, pp. 3522–3537, Dec. 2014.
[27] P. Maris Ferreira, C. Donche, A. Delalin, T. Quemerais, D. Gloria, T. Lasri, G. Dambrine, and C. Gaquiere, "Sub-fF 130 nm MOS varactor characterization using 6.8 GHz interferometry-based reflectometer," *IEEE Microw. Wireless Compon. Lett.*, vol. 25, no. 6, pp. 418–420, Jun. 2015.
[28] P. Maris Ferreira, C. Donche, E. Avignon-Meseldzija, T. Quemerais, F. Gianesello, D. Gloria, T. Lasri, G. Dambrine, and C. Gaquiere, "Fully integrated interferometry-based reflectometer for high-impedance instrumentation," *IEEE Trans. Microw. Theory Techn.*, vol. 66, no. 8, pp. 3901–3908, Aug. 2018.
[29] W. Qin and Q. Xue, "Complementary compact microstrip resonant cell and its applications to microwave Single- and dual-band bandpass filters," *IEEE Trans. Microw. Theory Techn.*, vol. 61, no. 2, pp. 773–781, Feb. 2013.
[30] S. Chen and Q. Xue, "A Class-F power amplifier with CMRC," *IEEE Microw. Wireless Compon. Lett.*, vol. 21, no. 1, pp. 31–33, Jan. 2011.
[31] Q. Xue, K. M. Shum, and C. H. Chan, "Low conversion-loss fourth subharmonic mixers incorporating CMRC for millimeter-wave applications," *IEEE Trans. Microw. Theory Techn.*, vol. 51, no. 5, pp. 1449–1454, May 2003.
[32] K. Man Shum, Q. Xue, and C. Hou Chan, "A novel microstrip ring hybrid incorporating a PBG cell," *IEEE Microw. Wireless Compon. Lett.*, vol. 11, no. 6, pp. 258–260, Jun. 2001.
[33] C.-L. Yang, C.-S. Lee, K.-W. Chen, and K.-Z. Chen, "Noncontact measurement of complex permittivity and thickness by using planar resonators," *IEEE Trans. Microw. Theory Techn.*, vol. 64, no. 1, pp. 247–257, Jan. 2016.
[34] A. Ebrahimi, J. Scott, and K. Ghorbani, "Ultrahigh-sensitivity microwave sensor for microfluidic complex permittivity measurement," *IEEE Trans. Microw. Theory Techn.*, vol. 67, no. 10, pp. 4269–4277, Oct. 2019.

SHICHANG CHEN (Member, IEEE) received the B.S. degree in electronic engineering from the Nanjing University of Science and Technology, in 2009, and the Ph.D. degree in electronic engineering from the City University of Hong Kong, in 2013.

From September 2013 to August 2014, he was a Postdoctoral Fellow with the City University of Hong Kong. He is currently an Associate Professor with Hangzhou Dianzi University. His research interests include high-efficiency power amplifier, integrated circuits, and sensors.

FENG ZHOU received the B.Eng. degree from Hefei University, Anhui, China, in 2018. He is currently pursuing the M.S. degree with a focus on microwave sensors and radar applications in Hangzhou Dianzi University.

KUIWEN XU (Member, IEEE) received the B.E. degree from Hangzhou Dianzi University, in 2009, and the Ph.D. degree from Zhejiang University, Hangzhou, China, in 2014. He was a Visiting Ph.D. Student with the National University of Singapore, Singapore, from 2012 to 2013. From 2014 to 2015, he was with Huawei Technologies Company Ltd. He is currently an Associate Professor with Hangzhou Dianzi University. His research interests include antenna design, microwave measurement, and electromagnetic inverse problems.

PENG ZHAO (Member, IEEE) received the B.Eng. and M.Phil. degrees from the Electronic Engineering Department, Zhejiang University, China, in 2006 and 2008, respectively, and the Ph.D. degree in electronic engineering from the City University of Hong Kong, China, in 2014. He is currently a Faculty Member with the Key Laboratory of RF Circuits and Systems of Ministry of Education, Microelectronics CAD Center, Hangzhou Dianzi University, Hangzhou, China. He is also with the State Key Laboratory of Millimeter waves, Southeast University, Nanjing, China. His research interests include microwave devices and computational electromagnetics.

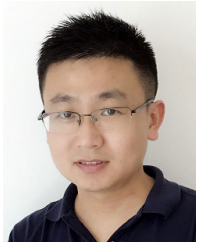

YANG YANG (Senior Member IEEE) was born in Bayan Nur, Inner Mongolia, China. He received the Ph.D. degree from Monash University, Melbourne, VIC, Australia, in 2013.

From July 2012 to April 2015, he was an Asia Pacific GSP Engineer at Rain Bird and a Global GSP Success Award holder of the year 2014. From April 2015 to April 2016, he has served as a Senior Research Associate at the Department of Engineering, Macquarie University, Sydney, NSW, Australia. From April 2016 to December 2016, he was a Research Fellow with the State Key Laboratory of Millimeter-Waves, City University of Hong Kong. In December 2016, he joined the University of Technology Sydney, Australia, as a Lecturer. His research interests include RFIC, microwave and millimeter-wave circuits and systems, reconfigurable antennas, wearable antennas, and wearable medical sensing devices and systems.

Dr Yang is a winner of CST University Publication Award 2018, by CST, Germany. He is currently an Associate Editor of IEEE Access.

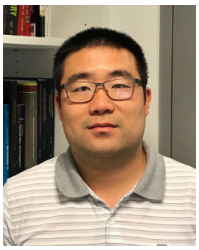

XI ZHU received the B.E. (Hons.) and Ph.D. degrees from the University of Hertfordshire (UH), Hertfordshire, U.K., in 2005 and 2008, respectively. He is currently a Lecturer with the School of Computing and Communication, University of Technology Sydney, Sydney, NSW, Australia. His research activities mainly involve in the areas of analogue baseband, radio frequency (RF), and mm-wave circuits and systems designs. He has coauthored over 80 refereed publications in the above-mentioned fields.

GAOFENG WANG (Senior Member, IEEE) received the Ph.D. degree in electrical engineering from the University of Wisconsin–Milwaukee, Milwaukee, WI, USA, in 1993, and the Ph.D. degree in scientific computing from Stanford University, Stanford, CA, USA, in 2001.

He was a Scientist with Tanner Research Inc., Pasadena, CA, USA, from 1993 to 1996. He was a Principal Researcher and a Development Engineer with Synopsys Inc., Mountain View, CA, USA, from 1996 to 2001. In 1999, he served as a Consultant with Bell Laboratories, Murray Hill, NJ, USA. He was the Chief Technology Officer (CTO) of Intpax, Inc., San Jose, CA, USA, from 2001 to 2003. He was the CTO of Siargo Inc., Santa Clara, CA, USA, from 2004 to 2010. He was a Professor and the Head of the CJ Huang Information Technology Research Institute, Wuhan University, Wuhan, China, from 2004 to 2013. He was the Chief Scientist with Lorentz Solution, Inc., Santa Clara, from 2010 to 2013. He is currently a Distinguished Professor with Hangzhou Dianzi University, Hangzhou. He has authored over 160 journal articles and holds 22 patents. His current research interests include integrated circuit and microelectromechanical system design and simulation, computational electromagnetics, electronic design automation, and wavelet applications in engineering.